Chapter 4. ANALYTICAL ELECTRON MICROSCOPY: X-RAY ANALYSIS

Donald R. Peacor Department of Geological Sciences,
University of Michigan, Ann Arbor, Michigan 48109, U.S.A.

4.1 INTRODUCTION

Inelastic scattering of the electron beam by a sample gives rise to many effects, one of which is emission of x-rays whose energies are characteristic of the elements in the specimen. Figure 4-1 illustrates the principal components of an analytical system consisting of electron beam, sample, detector, and associated electronics system. Beam-specimen interaction gives rise to characteristic x-ray spectra that are detected with an energy dispersive spectrometer (EDS) system consisting of a Li-drifted Si detector and associated electronics. The resulting signal is processed through a multichannel analyzer (MCA) and stored in digital form. On-line display on a cathode ray tube (CRT) gives rise to spectra as shown in Figure 4-2. Modern systems are computer controlled with software that permits on-line identification of elements and their approximate proportions. Alternatively, spectra can be stored, retrieved at a later time, and analyzed with software that determines peak areas (intensities), makes appropriate corrections, and calculates compositions. Although chemical information can be obtained in many different ways using TEM/STEM, relatively complete chemical analytical data can be obtained only with such a system, and the process is therefore commonly referred to by the term analytical electron microscopy (AEM).

The marriage of x-ray detectors with TEMs, combined with advances in electron optics that permitted formation of scanning images and the development of STEMs, was a natural outcome of developing technology (see §1.2.2 for a description of TEM/STEM and dedicated STEMs). Primarily because of space limitations, energy dispersive spectrometers (EDS) rather than wavelength dispersive spectrometers (WDS) have been

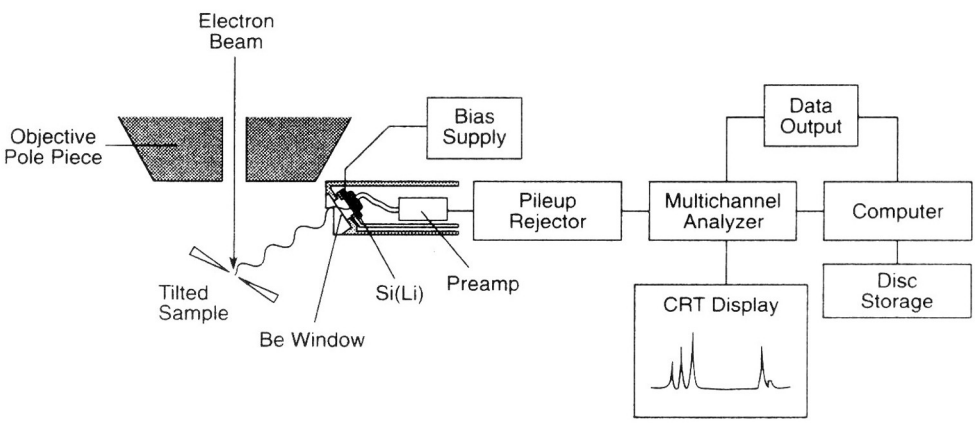

Figure 4-1. Principal components of an AEM system. Characteristic x-radiation and bremsstrahlung emitted by the sample is detected by an energy dispersive Si(Li) detector, collected in a multichannel analyzer, displayed on a cathode ray tube, and/or stored; computer software permits on-line or later analysis and display of spectra.

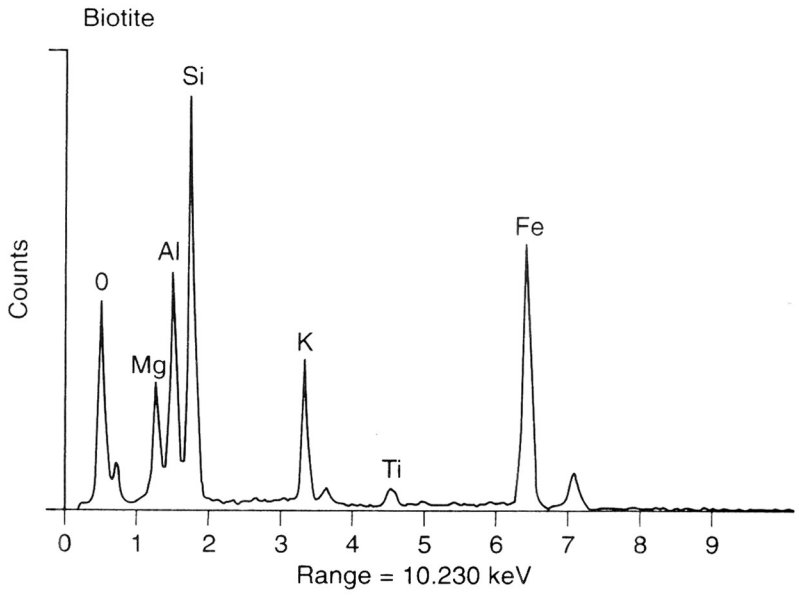

Figure 4-2. EDS spectrum of biotite. K_α peaks are labeled. Courtesy of W.-T. Jiang.

universally utilized. However, the first analytical instruments were little more than TEMs with spectrometers added without consideration of the special needs of such systems. They therefore gave rise to scattering of the beam with production of x-rays from areas of the specimen much larger than the effective beam diameter and from a great variety of scattering events in the column/specimen environment.

The early instruments ca. 1980 had two principal disadvantages: (1) the spectra were "dirty," with contributions from many sources other than the area of direct beam/specimen interaction, and (2) alignment of TEM/STEMs in TEM and STEM modes was separately carried out, so that shifts from one mode to the other were difficult and time-consuming, with resultant difficulty in recognition of areas in STEM mode that had been previously characterized in TEM mode. The recognition of the power inherent in combined TEM observations and accurate, high-resolution chemical analysis rapidly led to the development of TEM/STEM systems which were specifically engineered to optimize intensity, resolution, and sensitivity of x-ray spectra (i.e., a "clean" instrument) and, to provide easy transfer between TEM and STEM modes with direct correspondence between easily interpreted images. It is now possible to routinely obtain chemical analyses with resolutions approaching 20 nm whose quality approaches those obtained through electron microprobe analysis (EMPA).

The fundamental difference between electron microprobe analysis (EMPA) and TEM/STEM conditions is in the thickness of the sample. In EMPA the sample is thick enough to cause complete absorption of the incident beam; resultant spreading of the beam causes resolution to be approximately 2 μm. However, in TEM/STEM samples, little beam spreading occurs as the beam traverses the thin, electron-transparent sample. Advantages of EMPA include high precision and sensitivity and the ability to obtain absolute concentrations; however, EMPA data suffer from atomic number (Z), absorption

(A) and/or fluorescence (F) effects and have low point-to-point resolution. By contrast, STEM analyses have resolutions two orders of magnitude smaller than those of EMPA and usually require no ZAF corrections. However, they are of lower precision and sensitivity. The principal drawback however, is that absolute concentrations cannot be obtained; rather, only ratios of concentrations can be measured. Utilizing procedures introduced by Cliff and Lorimer (1975), mineral formulae are obtained by normalizing such ratios to a suitable absolute value. It is shown below that comparison of EMPA and TEM/STEM analyses of the same samples demonstrates that, under ideal circumstances, the quality of TEM/STEM analyses approach those of EMPA in most respects.

4.2 PRODUCTION OF X-RAYS

4.2.1 Inelastic scattering

Inelastic scattering, in which incident electrons lose energy, takes many forms. However, two processes dominate typical x-ray spectra as illustrated in Figure 4-2: (1) The continuous background, or "bremsstrahlung" radiation, and (2) The peaks superimposed on the background, each of which corresponds to an energy, or equivalent wavelength, that is characteristic of the element that gave rise to the radiation. Such peaks are therefore referred to as "characteristic" peaks. Their intensity, or peak area, is proportional to the concentration of the corresponding element in the sample.

The continuous background is produced by deceleration of incident beam electrons through interaction with the charge field of the atom core and inner-shell electrons of specimen atoms. A given loss of velocity for a specific electron corresponds to an energy loss which is converted into an x-ray photon of wavelength λ:

$$E = h\upsilon = hc/\lambda .$$

Specific energy losses can vary from zero to E_0, where E_0 is the full energy of an electron ($E_0 = eV$, where V is the acceleration potential) that loses all energy in a single scattering event. The high energy cutoff of continuous background therefore varies with E_0. Bremsstrahlung intensity gradually increases with decreasing energy, at an increasing rate as $E = 0$ is approached.

Characteristic x-radiation is produced by ionization of specimen atoms by the incident beam as shown in Figure 4-3. If the energy, E_0, of the incident beam electron exceeds the binding, or ionization, energy of an inner-shell electron of a specimen atom, the inner-shell electron may absorb energy equal to or greater than the ionization energy and thus be ejected from the atom. The result is an ionized atom with outer electrons in an unstable state. Resultant relaxation occurs by transition of outer electrons from high potential energy states to the energy level of the ejected electron. The excess energy ($E_L - E_K$, as shown in Fig. 4-3) may be converted to an x-ray photon with wavelength

$$E_L - E_K = h\upsilon = hc/\lambda.$$

Because the energy difference is quantized and characteristically different for each element, the energy, or wavelength, of the x-ray photon is characteristic of the element. Although it is not relevant to AEM, it should also be noted that relaxation can occur through ejection of an Auger electron rather than through production of an x-ray photon.

Ionized atoms may undergo many possible transitions as illustrated in Figure 4-4 for Fe, and as determined by selection rules. They are identified with the Siegbahn nomenclature which is, unfortunately, not entirely logically based on quantum number

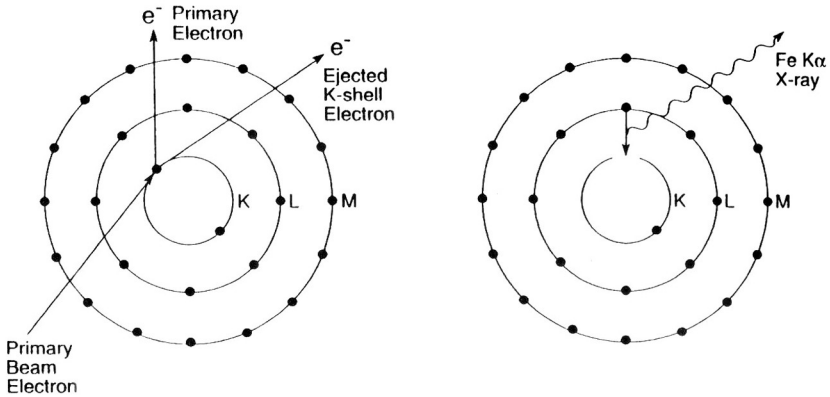

Figure 4-3. Production of characteristic x-radiation from an Fe atom. Transfer of energy of the primary beam electron (E_o) to a *K*-shell electron of Fe causes the *K*-shell electron to be ejected, leaving the Fe atom ionized. Replacement of the *K*-shell electron by an *L*-shell electron can give rise to a photon of x-radiation of energy E_L–E_K, labeled FeK_α (after Potts, 1987).

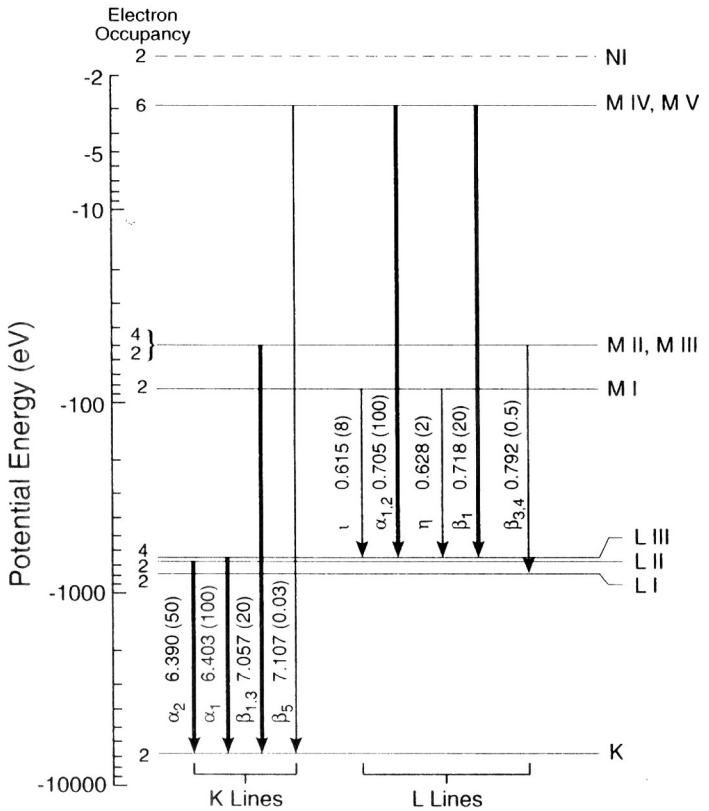

Figure 4-4. Characteristic emission lines of Fe. Relative intensities of lines are represented by the thickness of the arrows that represent electron transitions (after Potts, 1987).

considerations. As an example of the nomenclature, one Fe emission line is identified as FeK_{α_1}. The letter K identifies the K shell as having been ionized, and the symbol α corresponds to the energy level from which the replacing electron originated. The subscript 1 identifies a line that is one of two or more that are ordinarily observed as a single unresolved peak.

The energy of a given series of lines (e.g., K_α lines) increases as a linear function of Z^2 (Z = atomic number). Thus Z of the K_α lines in the EDS spectrum of Figure 4-2 increases from left to right. The energy of the lines of a given element decrease in the order $K > L > M$. Figure 4-4 illustrates the relative intensities of emission lines for Fe. The K_α line is always the strongest; they decrease in intensity in the orders: $I(K) > I(L)$...; $I(\alpha) > I(\beta)$...; $I(1) > I(2)$... .

Few of the many emission lines are useful in AEM for two reasons: (1) most are too weak to be observed or to give rise to count rates high enough to yield precise measurements, and (2) there are limits to the practical detection range of EDS spectrometers (> 20 keV), simply because the Li-drifted Si is largely transparent to higher energy radiation, although Ge detectors are now available with improved detector efficiences in the range 20-40 keV. The K_α lines of low atomic number elements are used as they are the most intense and are within the detectable range, whereas L lines are utilized for elements of intermediate Z.

The continuous radiation is generally undesirable as it must be subtracted from the spectrum before measurement of the areas of characteristic peaks. High backgrounds therefore diminish the precision of characteristic peak area measurements. The background may be perturbed by a variety of factors (see below) that cause errors in the subtraction process. It is therefore essential that both the peak area (intensity) and peak to background ratio (P/B) be maximized.

4.3 ENERGY DISPERSIVE SPECTROMETERS (EDS)

4.3.1 Integrated EDS system

Space limitations usually preclude the use of wavelength dispersive spectrometers (WDS) in TEMs, but solid-state x-ray detectors are ideal because of their compact size. Such energy dispersive spectrometers are efficient because of relatively large collection angles. They simultaneously detect a wide range of energies, generally sufficient to include the characteristic lines of most elements, as illustrated in Figure 4-2. Their principal disadvantages include: (1) poor energy resolution over most of their useful range compared to WDS, resulting in overlap of peaks that are typically completely separated in WDS. As a result, peak stripping functions are especially important in EDS. (2) Absorption of low energy radiation by the window of the detector results in inefficient detection of elements with Z < 11 (Na). Detectors have been designed to circumvent that problem. (3) Artifacts in the spectrum, as discussed below.

The principal component of a solid state detector is a crystal of Si containing traces of Li (Li-drifted Si crystal) as diagrammed in Figure 4-5. X-radiation entering the detector causes electron-hole pairs to be generated whose number is proportional to the energy of the radiation. The resulting charge pulse is amplified and stored in a channel of a multi-channel analyzer that is calibrated for the given charge (energy of incident radiation). Intensity of incident radiation is determined by the number of pulses

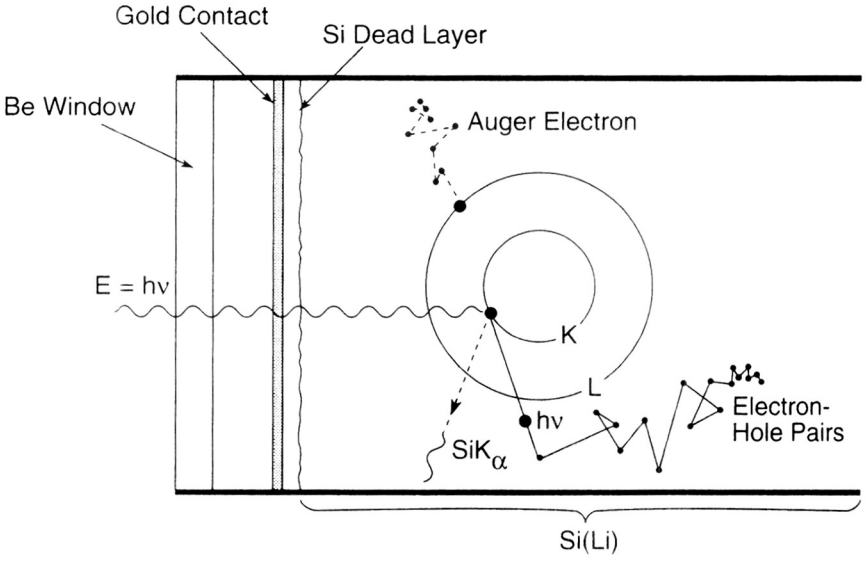

Figure 4-5. Representation of a part of a typical EDS detector, showing the Be window, gold contact layer, Si layer, and the Si(Li) crystal. The energy of the incident x-ray photon is dissipated in the crystal by a variety of inelastic interactions, the sum of which results in a pulse with current proportional to the energy of the incident photon (after Goldstein et al., 1981)

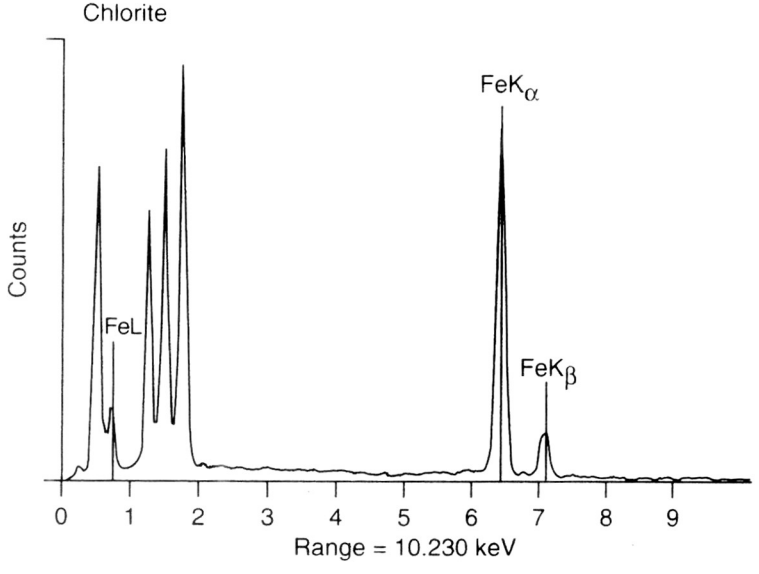

Figure 4-6. Typical EDS spectrum of chlorite, with characteristic Fe emission peaks labeled. Unlabeled peaks correspond, left to right, to O, Mg, Al, and Si. This spectrum was obtained using a Kevex *Quantum* detector. Courtesy of W.-T. Jiang.

accumulated in a given channel. When sufficient pulses have been obtained to define the spectrum, the contents of the MCA can be displayed on a CRT.

Modern spectrometer systems are computer-controlled with software that permits, among a wide range of options, immediate identification of all characteristic peaks, as shown in Figure 4-6, where the lines of Fe are identified. The contents of the MCA can be processed on-line or stored for later analysis. In either case, the manufacturer's software will have provision for processing the spectra by (1) subtracting the background curve that is primarily due to bremsstrahlung radiation, (2) "deconvolution" of overlapping peaks and determination of integrated intensities, (3) comparison of observed intensity ratios with those of standards in order to determine atomic ratios, and (4) calculation of normalized formulae from atomic ratios.

4.3.2 Types of detectors

The most common type of detector is constructed with a thin window of Be on the order of 10 μm thick in order to protect the crystal from contamination from the column environment. However, even such thin windows absorb incident x-radiation of low energy. The *K* lines of elements with $Z < 11$ are effectively entirely absorbed. Even NaK_α is significantly affected, with the result that peaks are severely diminished in intensity, with resulting imprecision in measurement of intensity; Na occurring in low concentrations may be entirely undetected. Although absorption of K_α lines decreases rapidly with increasing Z, the MgK_α, AlK_α, and SiK_α (Z = 12-14) are affected, and as they are characteristic emission lines of elements of critical importance in geological samples, the Be-windowed detector is not ideal.

The K_α lines of low atomic number elements are commonly measured with either a windowless or ultra-thin-window detector. Such detectors must be constructed with complex baffles to protect them from the atmosphere when not under vacuum. They are installed with low take-off angles, as is true for some other detectors, so that they can be placed near the specimen to give rise to as large a solid detection angle as possible, while avoiding the objective pole piece. They may be coupled with windowed detectors that are installed with high take-off angles, located above specially constructed objective pole pieces, and that are used for measurement of higher energy radiation.

Alternatively, relatively new windows made of a boron composite material have recently become available. Detectors with such windows can be installed at low angles to maximize solid detection angle and can be used for the full spectrum of energies. Nevertheless, even such detectors are relatively insensitive to radiation from low-Z elements, and results are only semiquantitative for O. Excellent results are obtained for Na, Mg, Al, and Si, however.

4.3.3 TEM/spectrometer systems

It is essential to obtain optimum count rates in order to cause measurements of integrated intensities to be precise, especially for *K* lines of low atomic number elements. For a given emission intensity, the count rate depends on two factors: (1) The active area of the detector, which is typically 30 mm^2, but may be as small as 10 mm^2 in early boron composite-window detectors. (2) Distance of the detector from the sample. The solid angle of detection is proportional to the inverse of the square of that distance. Efficient detection demands that it be optimized. That is accomplished by installation of the

detector axis normal, or nearly normal, to the electron beam. The detector can thus avoid the objective pole piece.

The take-off angle, as measured from the specimen surface to the detector, is an important parameter. If the counter is nearly normal to the electron beam and the specimen surface is normal to the beam, then x-rays produced in the sample must travel along relatively long paths before exiting the sample, and absorption is severe, even though ultra-thin samples are used. The sample must therefore be tilted toward the detector where detectors are oriented normal to the column. That is a time-consuming operation that may require specimen reorientation. On the other hand, as detector angles increase, interference with the pole piece requires that distance to sample be increased with resulting loss of counting efficiency. Take-off angles of approximately 20° are reasonable compromises.

High-angle, windowed detectors can therefore be permanently emplaced and utilized with horizontal samples, but must be combined with, say, ultra-thin-window detectors at low angles for light element detection. On the other hand, the single detector at low take-off angles, especially the mechanically-simple boron-composite windowed detector, is a great convenience in measuring the full range of x-radiation, but with the inconvenience of tilting the sample prior to analysis. A compromise in which the specimen need not be tilted can be achieved with a 20° take-off angle.

4.4 TEM/EDS SYSTEM CONCERNS

There are a number of factors that can cause x-rays to be generated outside of the area of direct beam-specimen interaction, or cause an increase in intensity or irregularities in background, or a decrease in intensity of characteristic peaks, and occurrence of detector artifacts. Although such factors are usually of little consequence in qualitative analysis, it is critical that the operator be aware of them and take appropriate precautions, especially as they may give rise to peaks of elements that are not in the sample. Three sources of problems are briefly discussed in this section: (1) spurious sources of radiation, (2) false peaks arising through the detector system, and (3) electron channeling.

4.4.1 Spurious sources of radiation

Characteristic and bremsstrahlung radiation can be produced at many sites within a TEM other than in the area of direct specimen-beam interaction. Those sources can be induced either by pre- or post-specimen environments.

Electrons that are poorly collimated can excite any area of a specimen. In addition, x-rays, principally bremsstrahlung, are produced in the C2 aperture (see Fig. 1-1) and can, if the aperture is thin enough, be transmitted to the specimen and excite emission of characteristic radiation. Such sources of spurious radiation can be detected using a "hole count," obtained by centering the beam on a small hole in an otherwise continuous specimen. Ideally, no counts should be obtained. Modern analytical instruments now normally have special apertures designed to minimize bremsstrahlung and have been engineered so that stray electrons have essentially been eliminated. It is essential that the correct analytical aperture be used during analysis, however.

Stray radiation is also produced through beam-specimen interaction, resulting in production of x-rays from many sources. There are three principal kinds of sources:

(1) Back-scattered electrons cause x-rays to be produced from the specimen chamber. (2) Incident beam electrons are scattered or diffracted into the post-specimen environment, causing direct production of x-rays, and back-scattered electrons. X-rays so-produced may be directly detected or may in turn cause fluorescence of lower energy x-radiation in the specimen. (3) The characteristic and bremsstrahlung radiation from the specimen itself cause fluorescence of x-rays from other areas of the specimen, or if the specimen is mounted on a grid, from the grid. Cu peaks are inevitable for samples mounted on Cu grids, a practical demonstration of production of x-rays from extraneous sources. For this reason, low atomic number grids (e.g., Be) that are readily available through commercial sources should be used for crushed grain mounts; the characteristic radiation so-produced cannot cause fluorescence of characteristic radiation in the sample. As the specimen is tilted to higher angles, such interaction becomes more significant. Some radiation of these kinds is unavoidable, although it can be minimized by construction of the specimen environment with low atomic number materials.

Tests for spurious sources of radiation, as well as of the effective diameter of interaction of beam and specimen, can be carried out using a thin specimen with two minerals of markedly different composition, but having an interface parallel to the beam, and with the area occupied by one approaching that of the effective beam diameter. Interaction of the beam with the latter phase should not give rise to x-rays from the former.

4.4.2 Detector system-related spectrum features

The EDS spectrum that is collected in the MCA and ultimately displayed should ideally contain only the characteristic peaks superimposed on the bremsstrahlung with an intensity distribution that is in direct proportion to the actual x-ray intensity distribution. Several processes inherent in the detection system give rise to changes in that ideal configuration. As illustrated in Figure 4-7, The most significant of these include: (1) escape peaks, (2) sum peaks, (3) asymmetry in background on the low energy side of peaks, and (4) background distortion due to high energy x-rays and back-scattered electrons.

The detector pulse caused by a photon of x-radiation that enters the detector may be activated by ionization of a *K*-shell electron of a Si atom. The ionized Si atom may relax through production of a photon of SiK_α radiation of energy 1.74 keV as shown in Figure 4-5. That photon is ordinarily absorbed before exiting the detector, in which case that energy is retained and counted as part of the original excitation event. However, the SiK_α photon may be lost from the detector. In that case, the energy retained is E(exc)-E(SiK_α), and a peak—called the escape peak—occurs in the spectrum at 1.74 keV less than that of the incident exciting radiation. That is, if MnK_α (E = 5.90 keV) enters the detector, a small escape peak will occur at (5.90-1.74) keV, in addition to the large peak at 5.90 keV. Such peaks are small, being on the order of magnitude of 1% of the principal characteristic peak. They may be erroneously attributed to trace amounts of some other element, however. They are generally subtracted from the spectrum in proportion to the intensity of characteristic peaks during standard spectrum processing.

Sum peaks occur at energies that are the sum of two of the energies of incident radiation. They occur when two photons that enter the detector at the same time cannot be differentiated by the counting circuitry, and are treated as a single photon. That is, if two SiK_α photons (E = 1.74 keV) were simultaneously counted, a small sum peak with E

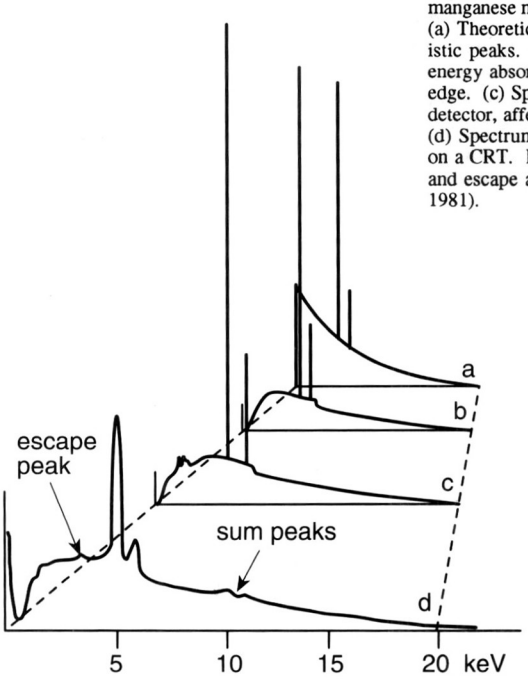

Figure 4-7. Illustration of the evolution of a spectrum of manganese metal, from specimen to CRT display. (a) Theoretical spectrum; bremsstrahlung and characteristic peaks. (b) Spectrum emitted by sample, with low energy absorption of bremsstrahlung and Mn-absorption edge. (c) Spectrum as x-radiation enters active Si(Li) of detector, affected by fluorescence and further absorption. (d) Spectrum as processed by electronics and displayed on a CRT. Energy distributions have been smeared out, and escape and sum peaks occur (after Goldstein et al., 1981).

$= 2 \times 1.74$ keV would occur. Such peaks are generally not observed in AEM owing to the low count rates from thin specimens.

Peaks are slightly asymmetric with enhancement of the low energy limb and with increased background. This is caused by loss of some of the energy of some incident photons during the detection process. Such "shelving" and "incomplete charge collection" give rise to a slightly enhanced background on the low energy side of the peak, with the effect decreasing to lower energy values.

The accelerating voltage used in a TEM is much higher than the value of approximately 15 kV that is typically used in an SEM or EMPA. The bremsstrahlung therefore has a high energy component that gives rise to Compton scatter in the Si of the detector, resulting in enhancement of the background at high energies. In addition, relatively high energy back-scattered electrons may enter the detector and cause distortion in the background. Both of these effects alter the background relative to its theoretical form.

There are two other minor features that ordinarily go unnoticed. One is a very small Si peak caused by fluorescence of a neutral layer of pure Si at the leading edge of the Li-drifted Si crystal. It would give rise to an apparent Si content of 0.2 wt % in a Si-free sample. The other is two absorption edges in the bremstrahlung spectrum. One is caused by a thin film of Au (used to apply a bias across the detector) on the Si crystal, and the other by Si itself. The latter is the result of the same process giving rise to the Si emission peak.

4.5 SPECTRUM ANALYSIS

4.5.1 Background subtraction

The final spectrum stored in the MCA consists of the characteristic peaks superimposed on the continuous bremsstrahlung that has been modified as described above. In order to obtain the integrated intensities of peaks it is necessary to remove the background. That is accomplished in one of two ways: (1) filtering, using a "top-hat" function, or (2) direct calculation of background.

The top hat filter is a function in which the counts in a series of adjacent channels of the MCA are averaged. The averaged value is assigned to the central channel. The series is shifted one channel and the process repeated until the entire spectrum has been traversed. The top hat actually has three sections, a central series of channels and two adjacent series. The filtered value is the difference between the average central value and the average side value. The filtered spectrum is a smoothed function in which linear sloping backgrounds are entirely suppressed. The advantage of such a method is that it is independent of the detailed specific aberrations in the spectrum, giving rise to a spectrum for which the peaks can be directly interpreted. Interpretation is normally carried out by comparison of filtered spectra with a set of stored "library" peaks.

Alternatively, the background can be calculated and subtracted from the experimental spectrum. The background is generally calculated for a specific region of the spectrum of interest and then normalized to the specific spectrum. In computerized systems using such functions, the calculated background curve in the area of interest can be directly superimposed on the spectrum displayed on the CRT. If the operator observes that it is apparently not at the proper level, the operator may adjust the relative vertical position of the background curve until an appropriate fit is obtained.

It is essential that manufacturer's software systems be tested using well-defined standards, and not treated as "black-boxes." We have recently found, for example, that software-generated backgrounds may be normalized to values that are too high where several characteristic peaks are adjacent, as for Na, Mg, Al, and Si. For example, the small Mg concentrations in Na-containing micas may be inaccurate by factors of 2 or 3.

4.5.2 Determination of peak intensities

It is a trivial matter to determine the integrated intensity of a peak that is entirely separated from other peaks. However, when peaks overlap, one of several different procedures must be used to unravel the combinations. These have such names as deconvolution, curve fitting, filtered least-squares fitting, etc.

So-called deconvolution may be accomplished by modeling the peaks of individual elements in terms of amplitude, width, and position. Such individual peaks can then be combined and compared with the overlapping peaks of the observed spectrum. The relative contributions of the separate contributions can be varied until a best fit is obtained. Alternatively, "library" spectra of the separate elements, with properly weighted consideration of the multiple lines occurring for a given element (e.g., K_α and K_β), can be directly compared with the observed spectrum, optimizing the fit. The operator chooses the elements for which the search is to be made based on a combination of an observation of the spectrum that usually results in identification of all elements of interest, or on knowledge of which elements are to be expected in the mineral being

analyzed. The result is a set of integrated intensities for each element that can be used in the determination of a normalized chemical formula. It is essential that the EDS spectrum energy scale be properly calibrated (an adjustment that can usually be made with peaks that occur at both the high- and low-energy region of the spectrum), so that the energy values for stored peaks may be correlated with the scale of observed spectra.

4.6 INSTRUMENTAL CONDITIONS

4.6.1 Instrument mode

It is, in general, possible to obtain EDS analyses in one of two ways: (1) In TEM mode by focusing the beam onto the area of interest. This technique gives the largest point-to-point resolution of several tens of nanometers. Beam damage can be minimized by defocusing the beam, but at the expense of a larger area of analysis. (2) In STEM mode in which the beam is focused to a fine probe whose size can be varied, but which can be on the order of 2.5 nm in diameter at the specimen. Analysis can be carried out with a stationary beam, or the beam can be rastered over the sample, with the length and width of the analyzed area controlled by the operator. One advantage of the method is that it permits the effects of the beam on any one point to be minimized, thus diminishing the effect of element diffusion (see below). In addition, element maps can be obtained (Fig. 4-8 below) for elements with relatively high concentrations, and compared with secondary, back-scattered, or transmitted electron images.

Operation in STEM mode was difficult in the earliest instruments, as they required separate alignments in TEM and STEM modes. Although features could be identified at a given site of a sample as viewed in TEM mode, transfer to STEM mode required lengthy alignment, commonly with loss of location in the specimen. The lens currents of modern computer-controlled STEMs can be stored, however, and transfer between TEM and STEM modes in well-aligned instruments requires only a few seconds.

4.7 METHODS OF DETERMINATION OF COMPOSITION

4.7.1 Cliff-Lorimer relation

The intensity of a given emission line emitted by a sample is proportional to the concentration, c_i, of a given element, with proportionality factors that relate to the physics of beam-sample interaction. In EMPA, the beam penetrates the sample to considerable depth, energy decreasing with penetration (Fig. 4-9). The intensity of x-ray production is therefore a function of atomic number (Z) effects (electron backscatter and retardation). The resulting emitted x-rays must pass through the sample and are subject to absorption (A) and fluorescence (F) effects. The observed intensity must therefore be corrected for these effects, each of which is a function, in part, of the composition of the sample.

However, in the thin electron-transparent films that are generally (but not always) used in AEM analysis, only a small proportion of the beam energy is lost through retardation in the sample and back scattering is inconsequential, so the beam may be considered to be of constant energy as it passes through the sample. Paths of emitted x-radiation from points of emission through the specimen to the surface are so short that absorption and fluorescence can usually be neglected.

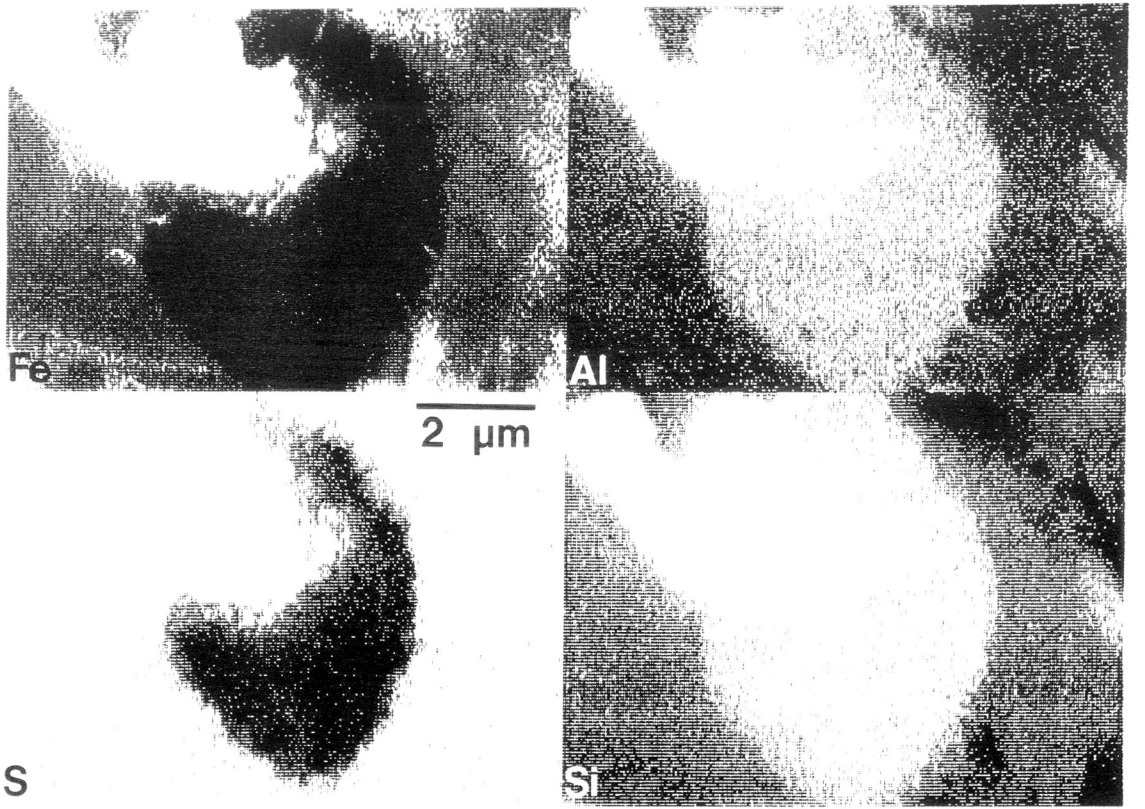

Figure 4-8. X-ray map of a pyrite framboid crystal in a matrix of illite, with the ion-milled thin edge bordering the upper left quadrant. The high Fe and S areas correspond to pyrite, but the upper left portion of the crystal has high Fe and no S contents, corresponding to magnetite that has replaced pyrite. The Si,Al-rich illite has a significant phengitic component as represented by the Fe map. Courtesy of W.-T. Jiang.

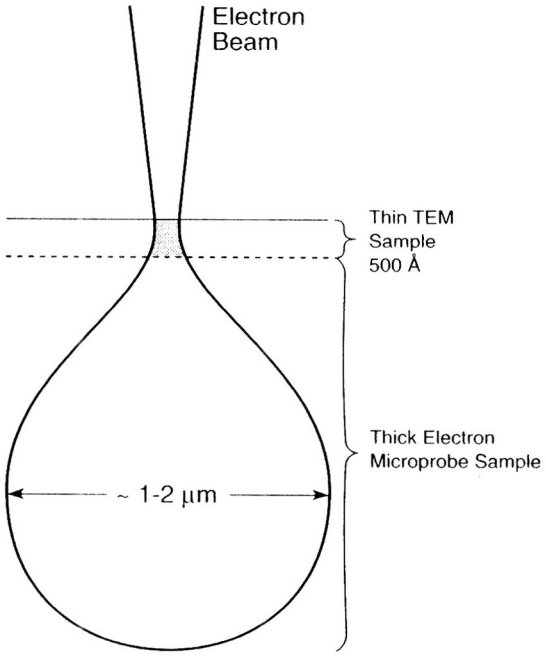

Figure 4-9. Diagram showing spreading of the electron beam within a thick electron microprobe or scanning electron microscope sample. Very little increase in effective beam width occurs for the first few tens of nanometers, corresponding to thin AEM samples. The analyzed area is thus only slightly larger than the beam diameter for AEM.

X-rays must penetrate the window of the detector, however, and are absorbed, especially in the case of K_α lines of low atomic number elements. In a standard Be-window detector, absorption occurs through the Be, a thin, dead layer of inactive Si, and a Au film. Note that if the same detector is used for standards and unknowns, the window absorption factor is negated.

Cliff and Lorimer (1975) applied these relations and formulated the equation:

$$c_a/c_b = k_{ab}(I_a/I_b)$$

where c_a and c_b are the atomic concentrations of elements a and b in a given compound, I_a and I_b are the intensities of emission lines of those elements, and k_{ab} is a proportionality factor that is a function of parameters concerned with beam/specimen interaction. If the compound contains only elements a and b, then absolute concentrations can be obtained by normalizing using the relation:

$$c_a + c_b = 1$$

If k_{ab} is experimentally determined for a standard compound of known composition, then the measured intensity ratio for a compound of unknown composition can be directly converted to a concentration ratio. The disadvantage of this technique is that absolute concentrations cannot be directly determined as they can by EMPA because the effective volume over which emission occurs cannot be determined. The principal advantage, however, is that ZAF corrections need not be applied as in EMPA, as the volume over which emission occurs is usually so small as to cause those factors to be inconsequential. Even where there is some ZAF effect, if the effects are for elements of similar atomic number, the effects largely are canceled through ratioing of the intensities.

4.7.2 *k*-values

It is traditional to determine the ratio of intensity of an x-ray line of a given element to that of Si because Si is the element most likely to occur in minerals, and its intensity

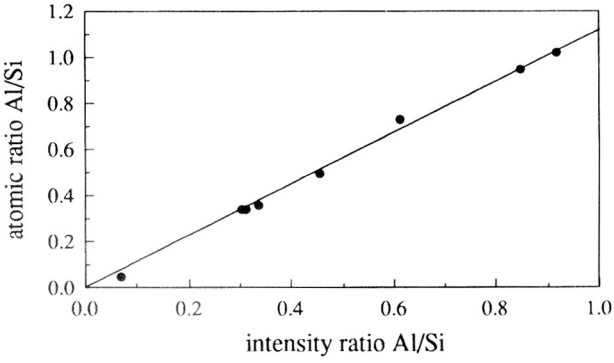

Figure 4-10. Plot of Al/Si atomic ratios versus measured Al/Si intensity ratios for several standards in the author's laboratory, with a least-squares-determined line fo best fit. The slope of the line is the k-value. Courtesy of W.-T. Jiang.

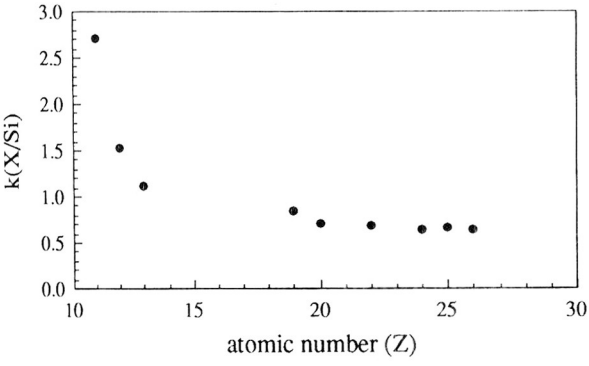

Figure 4-11. Plot of k-values ($k_{X,Si}$) used in the author's laboratory as a function of atomic number (Z) of element X. Courtesy of W.-T. Jiang.

can be accurately determined (as opposed to that of oxygen). It is possible to determine the intensity ratios for an element, say Al, in several standards having different ratios c_{Al}/c_{Si} (Fig. 4-10). The k-value, $k_{Al,Si}$ in this case, is determined by the slope of the line. The multiple determinations of k provide an internal check on the validity of the values (e.g., confirming that measurements were made in the true thin-film condition) as they should all plot on the same line.

The k values vary regularly as a function of atomic number. Figure 4-11 shows some values used in the author's laboratory. Where standards are not available for some element, approximate k-values can be obtained by interpolation between known values. If the concentration of the element in question is small, the resulting error in absolute concentration is negligible.

The k-values that are obtained by ratioing to Si can be used in the calculation of other k-values. The relation

$$k_{a,Si}/k_{b,Si} = k_{a,b}$$

can be used to calculate k-values for combinations of elements a and b that occur in the absence of Si.

4.7.3 Standardless analyses

The k-values are dependent on various instrumental factors, most notably beam potential, and thus vary with changes in electronics. The changes are small, however, and because they occur in an approximately proportional way for factors in both numerator and denominator of ratios, the k-factors are, for all intents and purposes, constants that can be stored and utilized long after they have been measured. This is valid

only for values obtained under specific conditions for a specific instrument. The one caveat to this has to do with the counter characteristics. Should the counter window or crystal be replaced, large changes in *k*-values are possible and standard *k*-factors must be redetermined.

Because the *k*-factors are permanently stored, they can be retrieved at the time of analysis and utilized to obtain concentration ratios in unknowns. Although intensity data for unknowns are processed using standard *k*-factors, no standardization is usually necessary at the time of analysis. Indeed, some use the term "standardless" for such AEM analyses for that reason, although the term is also used where the *k*-factors are calculated from first principles, as reviewed by Goldstein et al. (1986). Because data for standards need not usually be obtained, AEM analysis has a distinct advantage as compared with EMPA, for which much time is required for determination of standard data during the session in which analyses are obtained. Indeed, a small number of quantitative analyses can generally be obtained very quickly by utilizing crushed grains on formvar films on grids, as compared with the time required for EMPA. Rapid preparation of samples for which no polishing is required, combined with "standardless" analysis, gives rise to very rapid analysis.

There is one important exception to the general rule that data for standards need not be measured in a given session. That occurs when beam damage causes loss of an element from the beam-specimen interaction volume. Alkali elements, particularly K and Na, are especially subject to this problem. Special experimental techniques that are required are described below.

4.7.4 Normalization procedures

The concentration ratios obtained using the Cliff-Lorimer method must be normalized to some quantity in the chemical formula. It is common practice to normalize EMPA data to mineral formulae by normalizing to the numbers of O atoms in a standard formula unit, or to a number of O atoms that would be present if all anions such as OH were present as O. Thus, mica formulae may be normalized to 11 (or 22) O atoms (10 O + 2 OH pfu).

In the cases of minerals such as most olivines and orthopyroxenes for which there are few analytical problems, such a procedure may be appropriate. However, there may be uncertainties that cause such a procedure to give rise to misleading results: (1) Elements such as Fe may occur with more than one valence. Although valence can often be independently determined where analyzed volumes are large, the ultra-small volumes typical of AEM analyses negate even that procedure. (2) There is a tacit assumption that all elements have been accounted for in the analysis. Trace amounts of several elements may be unaccounted for, the levels of detectability being greater for AEM than EMPA. Light elements (e.g., N in NH_4) may remain undetected. (3) Diffusion may cause concentrations of alkali elements to be too low.

For those reasons, it is recommended that, whenever possible, normalization be carried out on the basis of some number of cations where such a space-group-determined number can reasonably be assumed on the basis of crystal chemical relations. For example, the sum of tetrahedrally-coordinated cations in alkali-containing tektosilicates is generally a constant, and normalization to such a value avoids the problem of alkali diffusion. In those structures that contain Fe, charge balance is subsequently obtained by adjusting the Fe^{3+}/Fe^{2+} ratio.

There is no convenient number of cations that is known on the basis of crystal structure refinements to be constant for some formulae. Amphiboles are particularly troublesome in that regard, for example, because of variation in A-site occupancy. Such problems are discussed for phyllosilicates in more detail in Chapter 9. In general, for those structures where there is some question about the constancy of some number of cations, normalization to cations introduces an error.

Thus, for structures such as amphibole where there may be both Fe^{3+} and Fe^{2+}, or Li that has not been detected, normalization to anions may be in error; however, because of ambiguity in A-site occupancy, normalization to cations is problematic for many, but not all, amphiboles. Each case must therefore be considered on its own merits, but it is essential that the choice of normalization be based on a full interpretation of the reasonable crystal chemical relations for the mineral in question while considering the analytical problems applicable to that mineral. Although I generally prefer cation normalization, there are many cases where anion normalization is preferable. In any event, normalization should not be automatically carried out with a single method, especially one that has been made available in "black box" computer software.

It is possible to compute weights percent from normalized formulae and to present an analysis in the form of oxides in the traditional fashion. Such a process is artificial however, and may be misleading for those who are not familiar with AEM techniques; it derives from analytical techniques for which individual weights percent represent directly observed data on an absolute scale, and for which standard errors can be easily estimated; by contrast, the errors associated with weights percent derived from AEM data are dependent on many assumptions in the normalization process in addition to the errors of analysis. Although it is seldom done, it is the concentration ratios that should normally be presented as the basic AEM data.

4.8 EXPERIMENTAL CONSTRAINTS

4.8.1 Specimen preparation

Samples of minerals are ordinarily prepared in one of three ways: (1) Fine particles spread on a formvar or C film over a metal grid. (2) Slicing with a diamond microtome, a process often used with clay mineral samples. (3) Ion milling, a process generally used when one wishes to retain original sample textures (see §1.6.2, this volume for detailed description).

The beam of high energy Ar ions not only removes atoms from the specimen surface, but damages the surface structure. Ar ions may be implanted in the surface, as frequently observed through a small Ar peak in EDS spectra of ion milled samples. More importantly, displaced surface ions may be reimplanted at small distances from original sites, resulting in apparent trace amounts of ions. The thinning rate varies with angle of the Ar beam to the surface, being greater at high angles. It is therefore advisable to thin rapidly at a high angle, but to change to a low milling angle or beam of lower energy at the end of thinning in order to minimize surface contamination. Because the sample is heated in the ion mill and therefore subject to damage, it may also be advisable to utilize sample cooling with liquid N_2.

4.8.2 Sample damage

The effects of direct atom displacement, ionization, and heating give rise to a variety

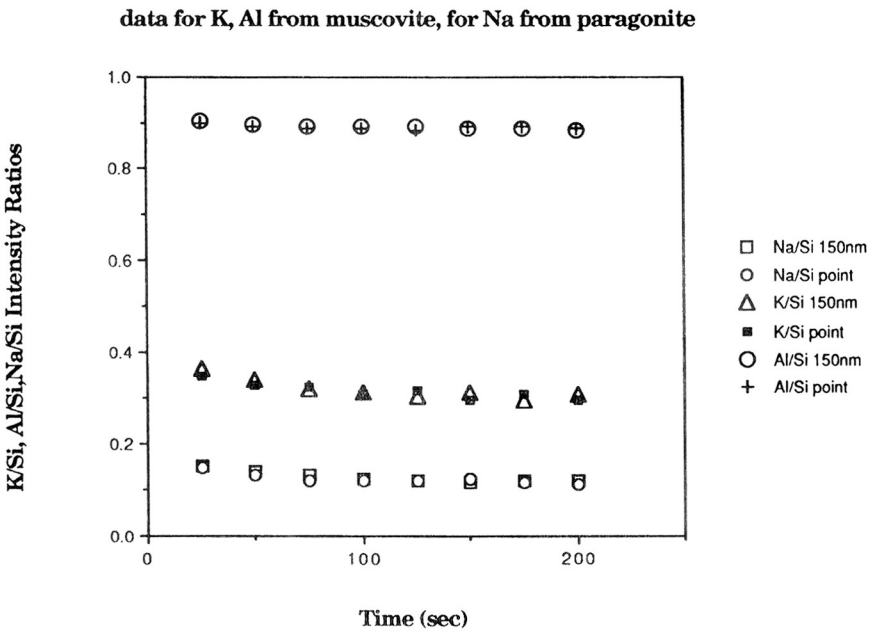

Figure 4-12. K/Si, Na/Si, and Al/Si intensity ratios for increasing time of analysis for constant beam and sample position. Data are plotted for both point (STEM mode) and 150 × 150 nm raster. The effect of diffusion (decreasing intensity) is large for K, intermediate for Na, and small for Al. Courtesy of G. Li.

of kinds of specimen damage that can cause serious AEM analysis errors. Figure 4-12 shows the variation in counts for K, Na, and Al relative to Si, obtained from ion-milled muscovite and paragonite with a stationary beam in STEM mode as a function of counting time. The change in count ratio is caused by diffusion, as can be detected by moving the beam to an area adjacent to beam-specimen interaction, where elevated counts are detected. The decrease in intensity is greatest for K, intermediate for Na, and smallest (but still measureable) for Al.

Figure 4-13 shows that the effect varies as a function of thickness. The data for K/Si and Al/Si counts were obtained with increasing distance from the edge of an ion-milled sample. Count rate increases because specimen thickness increases away from the edge. However, the K/Si intensity ratio continues to increase long after the Al/Si ratio has reached a constant value, implying that K diffusion occurs even for relatively thick samples.

Figure 4-13 also indicates that the intensity ratios vary as a function of area of analysis. At low count rates (thin edges), point analyses for both K (especially) and Al are subject to diffusion, whereas rasters 300 × 300 nm appear to be minimally affected by diffusion.

The effect increases with increasing count time, but sufficient counts must be obtained in order to optimize precision; thus, increasing accuracy (minimum diffusion) must be balanced against decreasing precision. In addition, the effects are minimized in relatively thick areas, but here too, accuracy is sacrificed due to absorption and fluorescence effects.

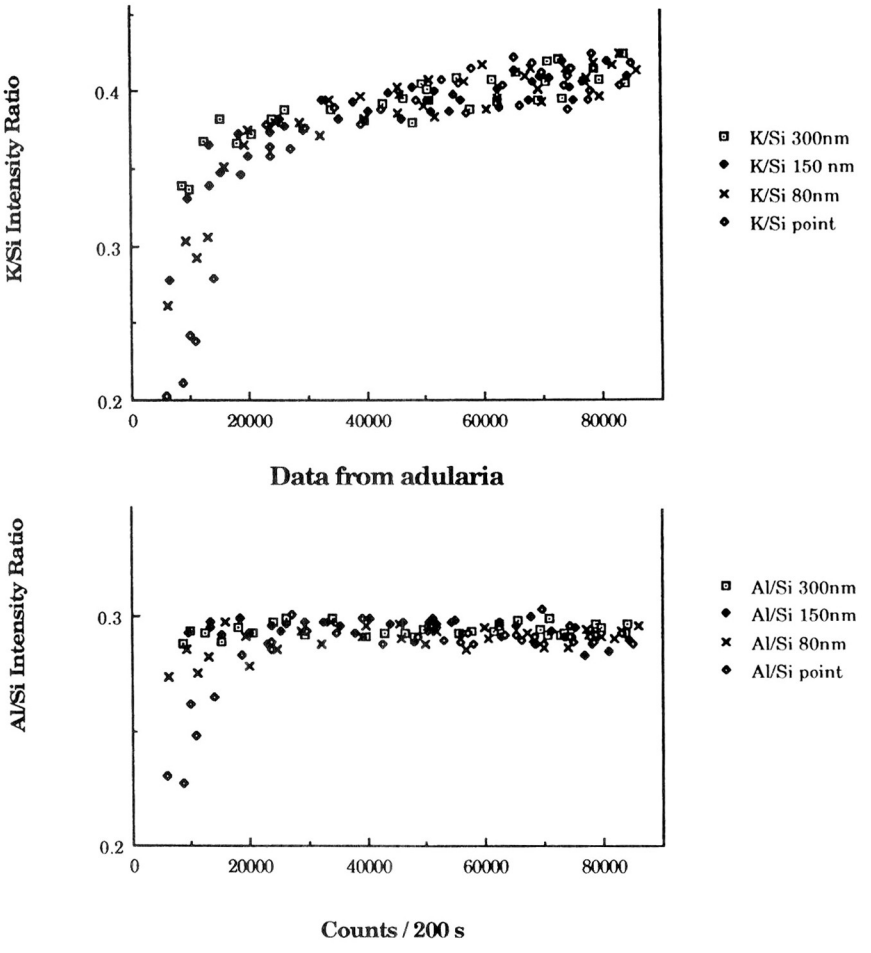

Figure 4-13. K/Si and Al/Si intensity ratios for increasing thickness of an ion-milled sample; increasing count rate is a measure of increasing thickness. The Al/Si intensity ratio approaches a constant, diffusion-free value, but that of K/Si is affected by K-diffusion at all thicknesses. Intensity ratios for different raster areas show that point analyses, especially, are subject to severe diffusion problems at very thin edges. Courtesy of G. Li.

These competing factors can be optimized by obtaining analyses in electron-transparent areas, but distant from ultra-thin edges in ion-milled samples, and by using a raster that is as large as possible with respect to the size of the grain to be analyzed and its relative homogeneity; the latter is determinable using a focused stationary beam in STEM mode, albeit in a qualitative way. If there is any doubt regarding the occurrence of diffusion, it should be validated by observing counts as a function of time; a decrease in number of counts per unit time may be ascribed to diffusion.

Mackinnon (1990) has shown how the rate of diffusion varies as a function of temperature. He showed that there was negligible diffusion of Na and Al in albite when a liquid N_2 stage was used, and he gave a detailed analysis of the effect. Diffusion can be approximately accounted for by obtaining data on a standard during the same work session and under the same conditions as for the unknown, the effects of diffusion being

canceled in the ratioing process. Because diffusion is thickness-dependent, count rates for both standard and unknown should be identical (assuming identical compositions), as an indicator of similar thicknesses, assuming identical microscope parameters. Because the effect is structure-dependent (and even orientation-dependent in micas) the standard used should be of the same structure type as the unknown. Serious errors in alkali contents can still occur in analyses of clay minerals such as smectite or illite, as the alkali diffusion rate is found, qualitatively, to be dependent on defect state. Thus, even muscovite, which is relatively defect-free, is an imperfect standard for the relatively defect-rich illites occurring in low-grade pelites.

4.8.3 Electron channeling

ALCHEMI (atom location using channeling-enhanced microanalysis) is a technique whereby the electron beam is concentrated on different levels of planes of indices hkℓ when a crystal is in diffracting condition for hkℓ, depending upon incident beam orientation (see §5.3 of this volume for a detailed discussion). Thus, if such alternate planes have different electron densities (e.g., consist of alternating planes of two different kinds of cations), the proportion of x-rays generated by one set of atoms or the other will depend on small differences in orientation. The technique is a useful one for determining ordering in alternate sites of certain phases. However, it can introduce serious errors into ordinary EDS analysis. Analyses should therefore always be carried out when the sample is not in a strong diffracting orientation.

4.8.4 Limits of thin film criterion

Goldstein et al. (1986) have reviewed the theoretical form of absorption and fluorescence corrections. Although they can be calculated to a first approximation, in practice such corrections are inaccurate. They do give an estimate of the relative significance of the corrections however. Such calculations show that absorption is by far the more significant factor, varying with absorption coefficient (which generally increases with increasing atomic number) and specimen thickness. The effective specimen thickness is in turn a function of tilt angle and sample shape. Absorption is significant primarily when one sample element has an absorption edge with energy slightly less than the higher energy emission line of another element. Absorption will occur through ionization of the inner shell corresponding to the absorption edge, causing emission (fluorescence) of characteristic radiation. Such absorption and emission occur for elements with atomic numbers slightly less than that of the element that gave rise to the initial emission radiation. High values of fluorescence for one element (lower atomic number) are thus correlated with high values of absorption for the higher atomic number element. The fluorescence correction factor is also a function of thickness.

In order to calculate correction factors for fluorescence and absorption, sample thickness must be determined. Measurements of thickness are difficult, time-consuming, and subject to error. Moreover, they must be made for each analysis point. The fluorescence and absorption functions are therefore best used with approximations of thickness to determine if absorption (or fluorescence) is significant; that is, approximate correction factors can be calculated for a given estimated composition in order to determine if they are significant within the precision of counting statistics. If correction factors are within precision as calculated with standard counting statistics, correction is not necessary.

It is much easier to make a simple, practical test of thin-film limits using ion-milled standards having continuously increasing thickness away from an edge, of known homogeneous composition, and with composition (and therefore absorption coefficient) similar to that of unknowns. Spectra should be measured in a traverse extending normal to the thin edge. Count rates should increase in proportion to thickness and, more importantly, intensity ratios should remain constant. As the thin-film criterion is exceeded, the rate of increase in count rate will diminish and intensity ratios change. The latter effect is best tested with intensity ratios involving both low- and high-energy lines, for which absorption would be optimally different; intensity ratios are minimally affected for an intensity ratio involving two emission lines of similar energy (assuming that absorption edges do not intervene) as for FeK_α and MnK_α, for example—a distinct advantage of the ratio technique. The operator rapidly becomes familiar with the qualitative relation between sample transparency and the thin film criterion for typical rock-forming silicates. Such measurements show that the the thin-film criterion is fulfilled for rock-forming silicates to limits of thickness of several tens of nanometers.

4.8.5 Limits of spatial resolution

A definition of spatial resolution is ambiguous because the limits of the beam itself are ill-defined. A practical definition is one based on inclusion of 90% of the generation of x-rays. Modern STEMs are capable of production of probes with effective diameters on the order of 2.5 nm. Nevertheless, even though beam spreading is minimized by the use of thin films, some beam spreading is inevitable, resulting in some loss of resolution. Beam spreading is a function of many variables, but the most important is specimen thickness. Various determinations of the effect indicate that order of magnitude broadening of 10 nm can be expected for mineral sample thicknesses of 100 nm.

Even 90% of x-ray production for areas with diameters on the order of magnitude of 10 to 20 nm may not be acceptable. A test of resolution can be carried out by utilizing a specimen containing two adjacent minerals having a boundary parallel to the beam, each with at least one significant element not present in the other. Calcite (Ca) and quartz (Si) are two such minerals. Counting for Ca, for example, should be carried out as the boundary is approached from the quartz side. As the calcite begins to interact with the limits of the beam, small amounts of Ca will be detected, with the amount increasing to a constant value when the beam is entirely within calcite. Such experiments indicate that resolutions on the order of 20 nm are possible in thin areas. Indeed, field emission STEMs have probe diameters as small as 1 nm with resultant resolution of a few nanometers.

4.8.6 Limits of sensitivity

Two factors determine the minimum detectable concentration of an element: (1) The presence of peaks that overlap the peak of interest or other factors that locally affect the background in the region of the spectrum that is of interest. Such factors were discussed above. Discussion of minimum detectable concentrations generally are made with the assumption that there are no overlapping peaks and background is a smooth, easily interpretable function. (2) As the concentration of a given element decreases, a point is reached at which the peak can no longer be discriminated from the background. The minimum concentration that can be detected is therefore determined by a statistical analysis of the precision with which such a peak can be detected.

X-ray counts obey Gaussian statistics; the standard deviation, σ, of a given number of counts, N, is given by $\sigma = \sqrt{N}$. At the 3σ confidence level, it is therefore necessary that

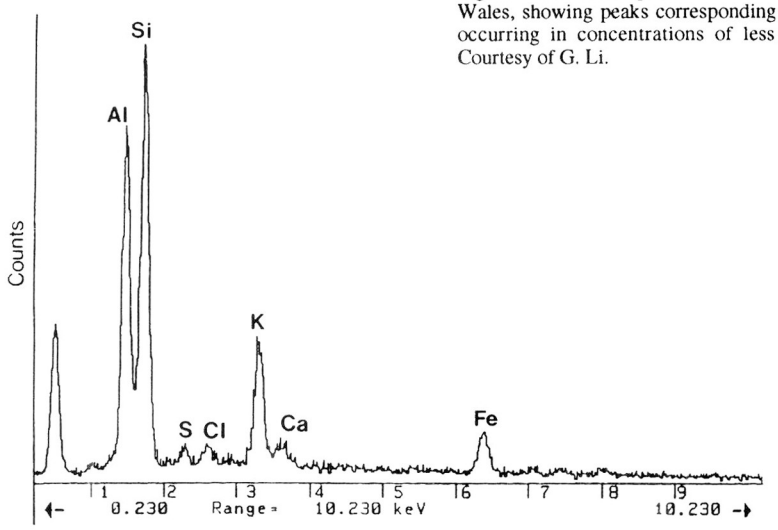

Figure 4-14. EDS spectrum of illite in a shale from Wales, showing peaks corresponding to S, Cl, and Ca occurring in concentrations of less than 0.5 wt %. Courtesy of G. Li.

the number of counts in a peak be greater than $3\sqrt{N}$. As the number of counts, N, increases, the relative error, $3\sqrt{N}/N$, decreases.

The minimum concentration is therefore determined by the following three parameters: (1) counting time, which should be maximized in order to minimize relative error within the bounds of convenience, sample damage, and sample position. (2) Peak counting rate, as determined by sample thickness and beam current. The need for high count rates must be balanced against absorption and specimen damage. (3) Peak-to-background ratio; subtraction of background from (peak + background) gives rise to an error in the peak intensity that is greater for higher backgrounds. For a given accelerating voltage, this is optimized at high take-off angles.

The actual limits of detection are best determined in a practical way by measuring intensity for a given element with decreasing concentration or with decreasing count times and peak count rates for low levels of concentration. Whereas EMPA data generally have minimum detection limits in the range of 0.01 to 0.1 wt %, AEM data are usually assumed to have limits on the order of a few tenths of one wt %. The latter value is valid for instruments designed several years ago, but modern instruments are capable of much better performance. Figure 4-14 exemplifies analysis for a sample with very small concentrations of several elements. The sample was muscovite from a Welsh slate, with small, but unusual S, Ca, and Cl peaks, and with minor amounts of Ti, and Cr. The S, Ca, and Cl are not generally expected in muscovite but were validated in several ways as occurring in this case. The formula obtained from a single analysis is

$$\left(K_{1.77},Ca_{0.15}\right)_{1.92}\left(Al_{3.37},Fe^{3+}_{0.55},Cr_{0.05},Ti_{0.03}\right)_4\left(Si_{6.01},Al_{1.99}\right)_8O_{20}\left(OH_{3.74},Cl_{0.19},S_{0.07}\right)_4.$$

The calculated wt % of S is 0.26%. Figure 4-14 shows that the minimum detectable limit is considerably below that value. In addition, the small but measurable Ti and Cr peaks correspond to 0.31 and 0.47 wt %, respectively.

Measurements such as the latter clearly show that AEM is routinely capable of detecting amounts on the order of 0.1 wt %, although for low atomic number elements

($Z < 10$) that limit is much larger. Nevertheless, the detection limits for most elements of geological significance now approach those typical of EMPA, with a limit near 0.1 wt %.

4.8.7 Accuracy and precision

The precision of a value of concentration of a given element relative to that of Si, c_a/c_{Si}, is determined simply by statistical relations based on the Cliff-Lorimer relation, where

$$c_a/c_{Si} = k_{a,Si} \times (I_a/I_{Si}) .$$

The standard error in c_a, $\sigma(c_a)$, is therefore the sum of the standard errors in $k_{a,Si}$, I_a, and I_b. The errors in k-values can be measured to relative precisions of better than ±1% if multiple standards are used, and especially if least-squares analysis is used to obtain k-values. The precision of the relative concentrations can then be readily calculated on the basis of counting statistics. Such standard errors are a normal component of the output of interpretation of spectra by commercial software. They in no way reflect accuracy, however.

Accuracy is affected by a number of factors, including beam-induced diffusion (especially of K; see above), absorption, and fluorescence. Because precision (total counts) increases with thickness, optimum conditions correspond to maximum thickness (assuming that the count-rate limit of the detector is not exceeded) as limited by the constraints of absorption and fluorescence. As with EMPA data, formulae should be normalized as soon as possible relative to the time of data measurement, as the basic requirement for analyses is that they produce formulae that are sensible relative to a known structure; possible errors should be detected at a time when they can be corrected. Such an initial test is available for EMPA data in that weights percent determined automatically just subsequent to analysis must sum to 100%, but AEM data can only be judged on the basis of the normalized formulae.

Tests of true accuracy of AEM results can best be obtained by data from standards. The relative accuracy of AEM data and the more familiar EMPA data can be determined from the same samples. Table 4-1 compares pyrophyllite and muscovite data as obtain-

Table 4-1. Structural formulae determined by EMPA and AEM of coexisting pyrophyllite, muscovite, and illite in Witwatersrand and Pennsylvania pelites.[1] (After Jiang et al., 1990)

	Witwatersrand, Republic of South Africa				Blackridge, Pennsylvania		
	Muscovite		Pyrophyllite		Muscovite	Pyrophyllite	NH_4-illite
	EMPA[2]	AEM[5]	EMPA[3]	AEM[5]	AEM[5]	AEM[5]	AEM[5]
Si	6.09(0.06)[4]	6.11(0.10)	7.96(0.04)	7.94(0.23)	6.09(0.16)	7.92(0.16)	6.37(0.27)
Al^{IV}	1.91(0.06)	1.89(0.10)	0.04(0.04)	0.06(0.23)	1.91(0.16)	0.08(0.16)	1.63(0.27)
Al^{VI}	3.93(0.08)	3.91(0.09)	3.99(0.02)	3.94(0.12)	3.54(0.13)	3.93(0.15)	3.78(0.31)
Ti	--	0.01(0.02)	--	--	0.06(0.01)	0.01(0.03)	0.01(0.02)
Fe	0.03(0.05)	0.03(0.02)	0.01(0.01)	0.01(0.01)	0.24(0.05)	0.04(0.03)	0.11(0.09)
Mg	0.03(0.02)	0.05(0.05)	0.01(0.01)	0.05(0.04)	0.16(0.06)	0.02(0.02)	0.10(0.11)
Ca	--	--	0.01(0.01)	--	0.02(0.03)	0.02(0.01)	0.02(0.03)
Na	0.21(0.03)	0.17(0.11)	0.01(0.01)	0.06(0.11)	0.04(0.01)	0.04(0.03)	0.03(0.04)
K	1.66(0.08)	1.72(0.19)	0.01(0.01)	0.04(0.07)	2.03(0.20)	0.05(0.05)	0.63(0.53)

[1]All formulae normalized to a total of 12 octahedral + tetrahedral cations.
[2]Average of 6 analyses.
[3]Average of 7 analyses
[4]Number in parentheses corresponds to two standard deviations.
[5]AEM analyses are from several rastered areas.

ed by EMPA and AEM for pyrophyllite and muscovite (see below for discussion). The AEM analyses have been converted to weights percent in order to facilitate comparison. The results show that the AEM-determined values for individual elements are identical to EMPA values, within error; i.e., the ranges of values for each of the methods are effectively the same. For those carefully obtained analyses, the accuracy of AEM results approaches that of the EMPA data. Although this example is for data for which special precautions were made, it nevertheless is not atypical of data that can be obtained with ordinary operating conditions.

4.9 APPLICATIONS

4.9.1 Qualitative exploratory analysis

The SEM is increasingly used in place of the optical microscope to characterize minerals in thin sections. Back-scattered electron images reflect differences in average atomic number of individual mineral grains, thus giving rise to contrast differences that permit easy definition of the individual grains. Once the contrast differences are defined, it is a simple matter to focus the beam on a given point or area having a specific contrast feature to obtain a qualitative EDS analysis. Experienced operators learn to recognize the spectra of specific minerals as surely as they can identify a mineral in hand specimen.

The AEM can be used in the same way for samples of rocks such as shales that consist of a variety of minerals with various textures, either in ion-milled samples or in fine-grained separates. As different areas are observed in TEM mode, contrast differences often lead directly to identification of given grains as being of interest. It is a simple matter to focus the beam on the area of interest and obtain an EDS analysis that generally is of sufficient quality to lead to immediate identification of the mineral in question. Figure 4-15 shows a low resolution TEM image of a shale for which contrast indicates the presence of an unusual mineral; the inset EDX spectrum immediately identifies it as florencite, a rare mineral, but one of great significance in this case because it is an important source of rare earth elements that are significant in Nd/Sm radioisotope systematics. Where there is ambiguity in identification based only on AEM data, as between iron oxides or polymorphs of TiO_2, additional data such as electron diffraction patterns can be immediately obtained. Alternatively, the operator may decide to switch to STEM mode if that option is available, in order to observe a scanning image, e.g., a transmitted electron image (TEI) or secondary electron image (SEI) image that displays contrast features that are different than those obtained in TEM mode. Areas with interesting contrast can immediately be qualitatively analyzed either with a stationary focused beam, or with a raster, with the resultant EDS spectrum leading directly to recognition of the mineral in question, as in an SEM. In either TEM or STEM mode, the sample can be rapidly surveyed until the operator is confident that all of the different minerals have been catalogued, and then the operator can proceed to focus on specific relations of interest.

4.9.2 Examples of analyses

4.9.2.1 Coexisting muscovite and pyrophyllite.

Jiang et al. (1990) studied coexisting pyrophyllite and muscovite in a low-grade pelite from Witwatersrand, South Africa. Both muscovite and pyrophyllite occurred as packets of layers in porphyroblasts that were large enough to analyze by EMPA, but fine-

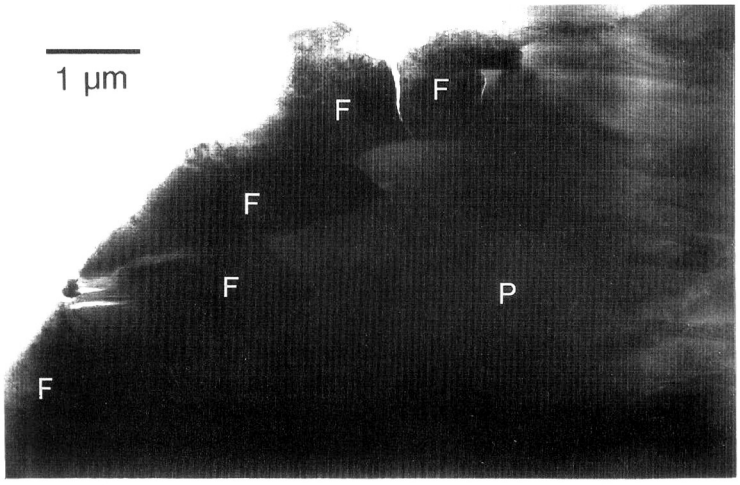

Figure 4-15. Low resolution TEM image of a shale from Wales, showing florencite, F, at an ion-milled thin edge in a matrix of phyllosilicates, P = chlorite plus illite. Courtesy of W.-T. Jiang.

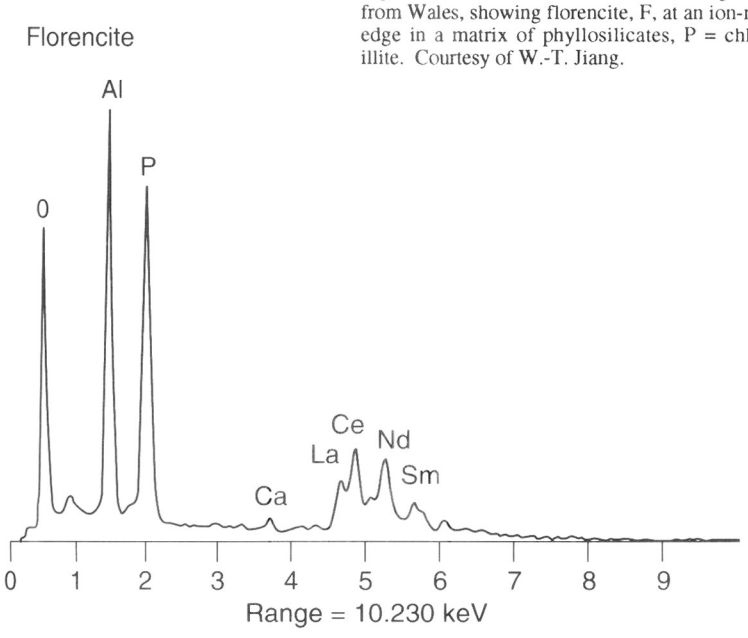

grained matrix material consisted of finely intergrown pyrophyllite and muscovite for which EMPA analyses inevitably showed overlap. Qualitative AEM analyses indicated that muscovite and pyrophyllite in both matrix and porphyroblasts were essentially identical in composition. Table 4-1 shows typical compositions as determined by electron microprobe for porphyroblasts and by AEM for matrix phases. The AEM analyses were obtained using a Philips CM12 instrument operated in STEM mode, with the beam rastered over less than 100 nm on an edge. All analyses are reasonable with respect to crystal chemical relations for such minerals; e.g., interlayer cation totals show minor deficiencies. The EMPA and AEM analyses for a single phase are identical within standard errors of individual elements. Analyses of coexisting muscovite, pyrophyllite, and NH_4-containing illite from a Pennsylvania slate are also given in Table 4-1. The Fe

and Mg (phengitic) components that preferentially occur in the muscovite are clearly indicated; by comparison the small amounts of Fe and Mg in the Witwatersrand muscovite, although at the limits of detectability, are probably real. The interlayer cation contents of the NH_4-illite are low only because no analysis could be obtained for N. Nevertheless, its presence is clearly indicated by low interlayer cation and charge totals. The high ^{IV}Si value, as compared to muscovite, is typical of metastable illite that formed early during diagenesis, whereas the muscovite has the nearly ideal composition typical of muscovite that formed under conditions of equilibrium.

4.9.2.2 Five-amphibole assemblage in blueschist

Smelik and Veblen (1989) described an assemblage of five coexisting amphiboles that occur within a blueschist from Vermont. The specific materials that were analyzed occur in an area of only approximately 100 μm of a thin section, demonstrating the high resolving power of the method, in combination with high resolution imaging. The results provide rather dramatic definitions of amphibole solvi. Smelik and Veblen utilized a Philips EM420 TEM fitted with a high resolution pole piece to minimize probe diameter, obtaining analyses in TEM mode.

Table 4-2 lists average normalized chemical formulae, obtained by normalizing to 23 O atoms, and assuming all Fe is Fe^{2+}. The glaucophane is a relatively coarse primary mineral, with an inclusion of and rimmed by calcic amphiboles. Some of the originally heterogeneous glaucophane contained no lamellae, whereas some exsolved locally to cummingtonite in lamellae no wider than 50 nm, and some exsolved to winchite lamellae. The analyses, apparently without significant overlap, demonstrate the minimal point to point resolution. Formulae of the glaucophane associated with exsolved cummingtonite and winchite are very similar to that of the unexsolved glaucophane, demonstrating that exsolution was controlled by local variations in original glaucophane composition. The calcium-amphiboles consist of actinolite and hornblende, demonstrating a solvus between those phases. Even though the normalized analyses must be in error to some degree based on the assumption that all Fe is Fe^{2+}, the analyses are all very reasonable in terms of normal amphibole crystal chemical relations, and demonstrate the near-probe accuracy of the average formulae.

4.9.2.3 Chlorite and white micas in shales

The ability of AEM to provide accurate analyses and to differentiate between compositions of different populations of the same mineral are illustrated by a recent study of Li et al. (in prep.) of a shale sample from central Wales. The shale had been subjected to anchizonal metamorphic conditions; i.e., it had been weakly metamorphosed to a Kubler crystallinity index of 0.35°2θ, but not to the point where slaty cleavage had developed, as had occurred in equivalent higher grade rocks.

The sample has three populations of phyllosilicates: (1) Grains with a detrital shape up to tens of microns in diameter, of two types: one is referred to as "stacks" and consists of alternating packets of chlorite and white mica; the other consists only of white mica. (2) Fine-grained, intergrown, matrix illite and chlorite occurring in two populations: one has {001} subparallel to bedding and is authigenic in origin; the other is oriented preferentially parallel to a developing slaty cleavage direction and was derived from the first kind by dissolution and crystallization. (3) Irregular fracture-fillings of mica, cross-cutting stacks.

Table 4-2. Average amphibole compositions from AEM for five-amphibole assemblage from Tillotson Pond area, northern Vermont. (After Smelik and Veblen, 1989)

		Unexsolved	Glaucophane Cum. host	Win. host	Cummingtonite	Winchite	Actinolite	Hornblende
Tetrahedral	Si	7.908	7.934	7.891	7.906	7.629	7.542	6.938
	Al	0.092	0.057	0.109	0.094	0.371	0.458	1.062
Total	T site	8.000	8.000	8.000	8.000	8.000	8.000	8.000
Octahedral	Al	1.592	1.452	1.613	0.149	1.162	0.465	0.713
M1, M2, M3	Ti	0.003	0.001	0.007	0.006	0.001	0.004	0.007
	Mg	2.132	2.252	2.201	3.732	2.733	2.949	2.380
	Fe^{2+}	1.272	1.294	1.179	1.112	1.104	1.582	1.900
	Mn	0.000	0.000	0.000	0.000	0.000	0.000	0.000
Total	M1-M3	5.000	5.000	5.000	5.000	5.000	5.000	5.000
Octahedral	Ca	0.234	0.232	0.311	0.590	0.742	1.678	1.640
M4	Na	1.678	1.603	1.604	0.232	1.021	0.275	0.269
	Fe^{2+}	0.085	0.163	0.081	1.153	0.235	0.042	0.086
	Mn	0.002	0.001	0.003	0.025	0.002	0.006	0.006
	Mg	0.000	0.000	0.000	0.000	0.000	0.000	0.000
Total	M4	2.000	2.000	2.000	2.000	2.000	2.000	2.000
A site	Na	0.160	0.197	0.079	0.152	0.205	0.242	0.571
	K	0.012	0.009	0.007	0.013	0.023	0.016	0.033
Total	A site	0.172	0.206	0.086	0.164	0.227	0.259	0.604
No. of analyses		12	9	10	14	6	6	10

Note: Formulae were normalized to 23 O atoms basis, and all Fe was assumed to be FeO. All analyses are from sample no. VTPI.

Table 4-3. Formulae derived from AEM and EMPA[1] analyses for chlorite and white mica in shale, central Wales. (Courtesy G. Li)

	Chlorite				White Mica						
	Detrital in stacks[2]		Matrix bedding-parallel	Matrix cleavage-parallel	Detrital in stacks		Detrital homogeneous		Matrix bedding-parallel	Matrix cleavage-parallel	Fracture filling
	AEM	EMPA	AEM	AEM	AEM	EMPA	AEM	EMPA	AEM	AEM	EMPA
Si	2.56	2.59	2.57	2.56	6.22	6.16	6.01	5.99	6.02	6.13	6.05
Al^{IV}	1.44	1.41	1.43	1.44	1.78	1.84	1.99	2.01	1.98	1.87	1.95
Al^{VI}	1.53	1.61	1.61	1.53	3.59	3.62	3.84	3.86	3.77	3.61	3.86
Ti	n.d.[3]	n.d.	n.d.	n.d.	0.07	0.03	0.03	0.01	0.01	0.04	0.01
Fe^{2+}	3.22	3.23	2.97	3.20	0.14	0.19	0.05	0.07	0.06	0.13	0.06
Mg	1.07	1.05	1.32	1.19	0.20	0.16	0.08	0.06	0.16	0.22	0.07
Mn	0.03	0.02	0.05	0.03	n.d.	n.d.	n.d.	n.d.	n.d.	n.d.	n.d.
Ca	n.d.	n.d.	n.d.	n.d.	n.d.	0.01	n.d.	n.d.	n.d.	n.d.	0.01
Na	n.d.	n.d.	n.d.	n.d.	n.d.	0.10	0.32	0.44	0.52	0.73	0.26
K	n.d.	n.d.	n.d.	n.d.	1.83	1.75	1.58	1.30	1.25	1.08	1.49

[1]All EMPA analyses are averages of 5 to 7 analyses.
[2]Stacks are grains with a detrital shape, consisting of parallel pockets of chlorite and mica.
[3]n.d. = not detected

Table 4-3 lists typical compositions of each of the five types of white mica and three kinds of chlorite, with compositions as determined by EMPA where grains were large enough for comparison. The AEM-determined compositions were obtained from single analyses obtained with a Philips CM12 instrument by rastering the beam over selected areas. Chlorite and white mica in "stacks" with detrital shapes were analyzed by both EMPA and AEM, providing direct comparison of the methods, although analyses were obtained from different grains for each method.

The chlorite in stacks is Fe-rich and interpreted to have formed through replacement of detrital biotite. Bedding-parallel chlorite, of lowest Fe content, was derived through authigenesis of detrital clays, and the cleavage-parallel chlorite developed during tectonic deformation through dissolution of bedding-parallel chlorite.

The mica in stacks is phengitic with significant Fe and Mg, and was inferred to have formed through crystallization in fissures produced by layer separations of biotite/chlorite during stress. Detrital mica has low Fe and Mg contents, but high values of Na in interlayer sites. Bedding-parallel mica has low phengite components, but with a high Na content inferred to represent metastable solid solution. The cleavage-parallel

mica consists of interlayered paragonite and muscovite that can not be resolved even by AEM, but is on average more phengitic than bedding-parallel micas. The mica that cross-cuts stacks was analyzed only by EMPA, and has relatively high Na and intermediate phengite contents.

4.10 CONCLUDING REMARKS

The techniques of analytical electron microscopy have been perfected over the last few years to the extent that compositions of rock-forming minerals can be routinely determined with accuracy and sensitivity that approach those of electron microprobe analyses. Quantitative analyses can be obtained with a spatial resolution that approaches 10-20 nm; the compositions of much smaller phases can be qualitatively determined. Under normal conditions, data for standards need not be obtained during a given session, so that analyses of individual minerals can be rapidly obtained. Lastly, in contrast to older instruments, modern computer-controlled TEM/STEMs offer a variety of easily-interpreted imaging systems with easy transfer from TEM to STEM mode. Compositions can be directly obtained from areas that are separately characterized by diffraction and high resolution microscopy. As was true of the process of improving EMPAs in the 1960s, AEM analytical techniques have now been improved to the point where they can routinely be used in the solution of petrological problems, especially in those cases where the resolving power of EMPA is inadequate.

ACKNOWLEDGMENTS

I am grateful to Peter Buseck for his efforts in making this *Reviews in Mineralogy* possible, and for the constructive reviews of R.L. Freed and two anonymous reviewers. I especially want to express my gratitude and appreciation to all of the many graduate students and colleagues who have contributed to the chemical analytical techniques of our laboratory, starting with Larry Allard, Dave Blake, Will Bigelow, and Drew Isaacs, and continuing with Jung Ho Ahn, Jung Lee, Lancy Yau, Yen Hong Shau, Wei-Teh Jiang, Gejing Li, and many others. They have been the real sources of expertise and creativity with respect to the AEM capabilities of our laboratory, and to them I will always be grateful. This project was supported by NSF Grant EAR-9104565.

REFERENCES

Cliff, G. and Lorimer, G.W. (1975) The quantitative analysis of thin specimens. J. Microscopy 103, 203-207.

Goldstein, J.I., Williams, D.B. and Cliff, G. (1986) Quantitative x-ray analysis. In Principles of Analytical Electron Microscopy, D.C. Joy, A.D. Romig Jr., and J.I. Goldstein, eds., Plenum Press, New York, 155-218.

Jiang, W.-T., Essene, E.J. and Peacor, D.R. (1990b) Transmission electron microscopic study of coexisting pyrophyllite and muscovite: Direct evidence for the metastability of illite. Clays and Clay Minerals 38, 225-240.

Mackinnon, I.D.R. (1990) Low-temperature analyses in the analytical electron microscope. In I.D.R. Mackinnon and F.A. Mumpton eds., CMS Workshop Lectures, vol. 2, Electron-Optical Methods in Clay Science. Clay Minerals Society, Evergreen, Colorado, 90-106.

Potts, P.J. (1987) Energy dispersive x-ray spectrometry. In A Handbook of Silicate Rock Analysis, P.J. Potts, ed., Chapman and Hall, New York, 286-325.

Smelik, E.A. and Veblen, D.R. (1989) A five-amphibole assemblage from blueschists in northern Vermont. Am. Mineral. 74, 960-964.

Williams, D.B. (1987) Practical Analytical Electron Microscopy in Materials Science. Philips Electronic Instruments, Inc. Electron Optics Publishing Group, Mahwah, New Jersy, 153 p.

Williams, D.B., Goldstein, J.I. and Fiori, C.E. (1986) Principles of x-ray energy-dispersive spectrometry in the analytical electron microscope. In Principles of Analytical Electron Microscopy, D.C. Joy, A.D. Romig, Jr., and J.I. Goldstein, eds., Plenum Press, New York, 123-154.